3D Flowerlike α-Nickel Hydroxide with Enhanced Electrochemical Activity Synthesized by Microwave-Assisted Hydrothermal Method

Linping Xu,[†] Yun-Shuang Ding,[‡] Chun-Hu Chen,[†] Linlin Zhao, Claire Rimkus,[§] Raymond Joesten,[†] and Steven L. Suib*[,†,‡]

Department of Chemistry, University of Connecticut, 55 N. Eagleville Rd., Unit 3060, Storrs, Connecticut 06269; Institute of Materials Science, 97 N. Eagleville Rd., Unit 3136, Storrs, Connecticut 06269; and Unit 2216, 21 Wellesley College Road, Wellesley, Massachusetts 02481-0222

Received August 6, 2007. Revised Manuscript Received November 2, 2007

Nickel hydroxide has received increased attention especially due to its electrochemical properties and potential applications in rechargeable Ni-base alkaline batteries, e.g., Ni/Cd, Ni/Zn, and Ni/MH. $Ni(OH)_2$ has a hexagonal layered structure with two polymorphs, α- and β-$Ni(OH)_2$. α-$Ni(OH)_2$ shows superior electrochemical properties compared to those of the β-form. Nanosized flowerlike α-nickel hydroxide materials with an interlayer spacing of 7.0 Å have been prepared by a microwave-assisted hydrothermal method. The experimental results from XRD and FT-IR showed that the $Ni(OH)_2$ sample prepared by this method had the typical α-phase. FE-SEM images showed many uniform flowerlike architectures with diameters of 700 nm−1μm which consisted of the aggregated flakes. TEM results showed the flakes were built up from many nanocrystals with 2–3 nm diameters. TGA and TPD were employed to investigate thermal stability and gas evolution during the heating process. α-Nickel hydroxide was transferred to NiO with a cubic crystalline structure after being calcined at 450 °C; the NiO still kept the morphology of α-$Ni(OH)_2$. Cyclic voltammetry was used to determine the electrochemical properties of the $Ni(OH)_2$ electrode in 1 M KOH. α-$Ni(OH)_2$ prepared by MW-HT had the best electrochemical activity for the electrochemical reduction of O_2 compared with α-$Ni(OH)_2$ synthesized by conventional HT methods and β-$Ni(OH)_2$. The effects of nickel sources and precipitators on the phase and morphology of the products were studied. Conventional hydrothermal methods were used to study the role of microwave irradiation. The possible growth mechanism is discussed here. The CV experiments showed that H_2O_2 can be reduced to OH^- on the α-$Ni(OH)_2$ electrode. The Levich equation was used to calculate the number of electrons transferred during the O_2 redox reaction.

1. Introduction

Nickel hydroxide has received increased interest because of its electrochemical properties and potential applications in rechargeable Ni-based alkaline batteries, e.g., Ni/Cd, Ni/Zn, and Ni/MH.[1–5] $Ni(OH)_2$ also has been used as a precursor for catalysts.[6] Nickel hydroxide has a hexagonal layered structure with two polymorphs, α- and β-$Ni(OH)_2$.[7–10] The β-form has a brucite-like structure, which has a hexagonal lattice and consists of an ordered stacking of well-oriented $Ni(OH)_2$ layers, without any intercalated species in the interlayer space. The interlayer distance is ∼4.6 Å. The β-form is a stoichiometric phase with a composition $Ni(OH)_2$. β-$Ni(OH)_2$ is a very active cathode.[5] α-$Ni(OH)_2$ is a hydroxyl-deficient phase with the hydrotalcite-like structure which consists of stacks of positively charged $Ni(OH)_{2-x}$ layers and contains intercalated anions and water molecules in the interlayer space to restore charge neutrality. The interlamellar distance is about 7 Å. The structure of α-$Ni(OH)_2$ displays more disorder because the layers are oriented randomly.

The composition of α-$Ni(OH)_2$ can be represented by the general formula $[Ni(OH)_{2-x}A^{n-}_{x/n}\cdot yH_2O]$ with $x = 0.2$–0.4, $y = 0.6$–1, and A = Cl^-, NO_3^-, SO_4^{2-}, CO_3^{2-}, or OCN^-.[10,11] Compared with β-$Ni(OH)_2$, α-$Ni(OH)_2$ shows superior electrochemical properties;[10] for instance, α-$Ni(OH)_2$, on oxidation, is converted to γ-NiOOH at a lower potential than the corresponding oxidation of β-$Ni(OH)_2$ to β-NiOOH. The large interlayer space is the distinguishing feature of α-$Ni(OH)_2$, which results in an interesting interlayer chemistry[12] and electrochemical activity.[13] However, α-$Ni(OH)_2$ is unstable and is hard to prepare since this phase

* To whom correspondence should be addressed. E-mail steven.suib@uconn.edu.
[†] University of Connecticut.
[‡] Institute of Materials Science.
[§] Unit 2216.

(1) Taniguchi, A.; Fujioka, N.; Ikoma, M. *J. Power Souces* **2001**, *100*, 117.
(2) Shukla, A. K.; Venugopalan, S.; Hariprakash, B. *J. Power Sources* **2001**, *100*, 125.
(3) Morioka, Y.; Narukawa, S.; Itou, T. *J. Power Sources* **2001**, *100*, 107.
(4) Wronski, Z. S. *Int. Mater. Rev.* **2001**, *46*, 1.
(5) Hu, W.; Gao, X.; Noréus, D.; Burchardt, T.; Nakstad, N. K. *J. Power Sources* **2006**, *160*, 704.
(6) Ovshinsky, S.; Feteenko, M. A.; Ross, J. *Science* **1993**, *260*, 176.
(7) Coudun, C.; Grillon, F.; Hochepied, J.-F. *Colloids Surf., A* **2006**, *280*, 23.
(8) Rajamathi, M.; Kamath, P. V.; Seshadri, R. *Mater. Res. Bull.* **2000**, *35*, 271.
(9) Mavis, B.; Akine, M. *Chem. Mater.* **2006**, *18*, 5317.
(10) Jeevanandam, P.; Koltypin, Y.; Gedanken, A. *Nano Lett.* **2001**, *1*, 263.
(11) Mavis, B.; Akine, M. *J. Power Sources* **2004**, *134*, 308.
(12) Rajamathi, M.; Subbanna, G. N.; Kamath, P. V. *J. Mater. Chem.* **1997**, *7*, 2293.
(13) Oliva, P.; Leonardi, J.; Laurent, J. F.; Delmas, C.; Braconnier, J. J.; Figlarz, M.; Fievet, F. *J. Power Sources* **1982**, *8*, 229.

10.1021/cm702207w CCC: $40.75
Published on Web 12/12/2007

changes rapidly to the β-form during synthesis or on storage in a strong alkaline medium.[11]

Control of the shape of inorganic nanomaterials has received increased attention due to its important role in influencing magnetic, electrical, optical, and other properties.[13–19] There are many factors which might affect the product shapes, such as the internal structure of the product, solvents used, temperature of preparation, concentration of the reactants, and the use of surfactant templates, etc.[10,20–22] Nanotubule α-$Ni(OH)_2$ has been obtained by urea precipitation in the presence of sodium dodecyl sulfate.[23] Hollow microspheres of β-$Ni(OH)_2$ were fabricated via a template-free approach in a strong alkaline solution of glycine.[19] Flowerlike Ni particles resulted from the hydrogen reduction of β-$Ni(OH)_2$ crystallites which served as the self-sacrificing templates.[14] Rb-OMS-2 and pyrolusite with flowerlike morphologies were made by a direct and mild reaction between rubidium chromate and manganese sulfate without any organic templates.[24]

Microwave irradiation heating is an alternative method for the synthesis and processing of these materials because of the low thermal gradients and reduced processing time.[25–29] With the assistance of microwave heating, sintering of ceramics has been found to be advantageous in the reduction of particle sizes, lowering of the sintering temperature, and shortening of firing times.[30] Microwave hydrothermal (MW-HT) methods have been known to have greater advantages from a kinetic perspective as compared to conventional hydrothermal processing of oxides.[31–35] The initial heating is rapid which can lead to energy savings. Barium titanate[36] was synthesized by a MW-HT method: Compared to conventional hydrothermal heating, MW hydrothermal methods were better as regards saving of time, lowering required temperatures, and easy application. The obtained $BaTiO_3$ powder had a monosized distribution of equiaxial particles of dimensions of 50 nm. The MW-HT method has been widely used to prepare metal powder.[37–40]

There are several methods to synthesize α-$Ni(OH)_2$, such as precipitation, electrochemical impregnation, and the "chimie douce" technique.[41–43] Because the pH of the solution remains relatively low throughout the reaction in the presence of urea, this method offers an excellent opportunity to prepare α-$Ni(OH)_2$.[10] Jeevanandam et al.[10] attempted to synthesize nanosized α-$Ni(OH)_2$ with good stability in KOH by utilizing ultrasonic radiation in the urea system. Zhao et al.[44] succeeded in obtaining α-$Ni(OH)_2$ by a homogeneous precipitation method with urea. Sometimes mixtures of α- and β-$Ni(OH)_2$ were produced which were easily converted to β-$Ni(OH)_2$ after aging in alkaline media. Nanocrystalline α-$Ni(OH)_2$ materials with morphologies of spherical agglomerates were prepared from aqueous solution by decomposition of urea.[45] Cao reported that α-$Ni(OH)_2$ with dandelion-like nanostructures was obtained with the reverse microemulsion method.[46] Nanowhisker α-$Ni(OH)_2$ was prepared by precipitation method in which ammonia was used as precipitator.[47]

Electrochemical reduction of oxygen is a reaction with prime importance due to practical applications in fuel cells, metal−air batteries, and energy-saving brine electrolytic processes.[48] Oxygen reduction possibly takes two pathways: (1) four-electron transfer process of O_2 to OH^-; (2) the two-electron pathway which involves produce of hydrogen peroxide and decomposition of peroxide.[49,50] Four-electron reduction is the ultimate goal to improve the efficiency of the full cell or battery. The pathway of oxygen reduction is strongly dependent on the electrode materials. So far, the most effective catalysts used to promote oxygen reduction reactions are Pt-based materials, highly dispersed on the substrate with high surface area, which are very expensive. The main challenge is to develop high active catalysts for O_2 reduction to OH^- which are efficient enough to replace

(14) Ni, X.; Zhao, Q.; Cheng, J.; Zheng, H.; Li, B.; Zhang, D. *Chem. Lett.* **2005**, *34*, 1408.
(15) Guan, X.; Deng, J. *Mater. Lett.* **2007**, *61*, 621.
(16) Li, B.; Xie, Y.; Wu, C.; Li, Z.; Zhang, J. *Mater. Chem. Phys.* **2006**, *99*, 479.
(17) Zhou, G.; Yao, Q.; Wang, X.; Yu, J. C. *Mater. Chem. Phys.* **2006**, *98*, 267.
(18) Wang, D.; Song, C.; Hu, Z.; Fu, X. *J. Phys. Chem. B* **2005**, *109*, 1125.
(19) Wang, Y.; Zhu, Q.; Zhang, H. *Chem. Commun.* **2005**, *41*, 5231.
(20) Li, X.; Liu, J.; Li, Y. *Mater. Chem. Phys.* **2003**, *80*, 222.
(21) Liu, X.; Lan, Y. *Mater. Lett.* **2004**, *58*, 1327.
(22) Liu, X.; Qiu, G.; Wang, Z.; Li, X. *Nanotechnology* **2005**, *16*, 1400.
(23) Liu, H.; Peng, T.; Zhao, D.; Dai, K.; Peng, Z. *Mater. Chem. Phys.* **2004**, *87*, 81.
(24) Li, W.-N.; Yuan, J.; Gomes-Mower, S.; Sithambaram, S.; Suib, S. L. *J. Phys. Chem. B* **2006**, *110*, 3066.
(25) Tsuji, M.; Hashimoro, M.; Tsuji, T. *Chem. Lett.* **2002**, *31*, 1232.
(26) Reguera, E.; Díaz-Aguila, C.; Yee-Madeira, H. *J. Mater. Sci.* **2005**, *19*, 5331.
(27) Prada, C.; Morán, E. *Chem. Mater.* **2006**, *18*, 2719.
(28) Kalyani, P.; Kalaiselvi, N.; Renganathan, N. G. *J. Power Sources* **2003**, *123*, 53.
(29) Giri, J.; Sriharsha, T.; Bahadur, D. *J. Mater. Chem.* **2004**, *14*, 875.
(30) Swain, B. *Adv. Mater. Process.* **1989**, *134*, 76.
(31) Komarneni, S.; Pidugu, R.; Li, Q. H.; Roy, R. *J. Mater. Res.* **1995**, *10*, 1687.
(32) Topsett, G. A.; Conner, W. C.; Yngvesson, K. S. *ChemPhysChem* **2006**, *7*, 296.
(33) Zhang, Q. H.; Luo, J.; Vileno, E.; Suib, S. L. *Chem. Mater.* **1997**, *9*, 2090.
(34) Zhang, Q. H.; Suib, S. L. *Chem. Mater.* **1999**, *11*, 1306.
(35) Malinger, K. A.; Laubernds, K.; Son, Y.-S.; Suib, S. L. *Chem. Mater.* **2004**, *16*, 4296.
(36) Guo, L.; Luo, H.; Gao, J.; Guo, L.; Yang, J. *Mater. Lett.* **2006**, *60*, 3011.
(37) Tsuji, M.; Hashimoto, M.; Nishizawa, Y.; Kubikawa, M.; Tsuji, T. *Chem.—Eur. J.* **2005**, *11*, 440.
(38) Tsuji, M.; Hashimoto, M.; Nishizawa, Y.; Tsuji, T. *Chem. Lett.* **2003**, *32*, 1114.
(39) Tsuji, M.; Hashimoto, M.; Nishizawa, Y.; Tsuji, T. *Chem. Lett.* **2004**, *33*, 370.
(40) Liu, F.; Chang, Y.; Ko, F.; Chu, T. *Mater. Lett.* **2004**, *33*, 474.
(41) Diyit, M.; Kamath, P. V.; Gopalakrishnan, J. *J. Electrochem. Soc.* **1999**, *146*, 79.
(42) Liu, B.; Wang, X. Y.; Yuan, H. T.; Zhang, Y. S. *J. Appl. Electrochem.* **1999**, *29*, 853.
(43) Jayashree, R. S.; Kamath, P. V. *J. Appl. Electrochem.* **1999**, *29*, 454.
(44) Zhou, Y. L.; Wang, J. M.; Chen, H.; Pan, T.; Zhang, J. Q.; Cao, C. N. *Int. J. Hydrogen Energy* **2004**, *29*, 889.
(45) Akinc, M.; Jongen, N.; Lemaitre, J.; Hofmann, H. *J. Eur. Ceram. Soc.* **1998**, *18*, 1559.
(46) Cao, M.; He, X.; Chen, J.; Hu, C. *Cryst. Growth Des.* **2007**, *7*, 170.
(47) Zheng, M.; Cao, J.; Chen, Y.; Ma, X.; Deng, S.; Tao, J. *Chem. Lett.* **2005**, *8*, 1174.
(48) Villers, D.; Jacques-Bedard, X.; Dodelet, J. *J. Electrochem. Soc.* **2004**, *156*, A1507.
(49) El-Deab, M. S.; Sotomura, T.; Ohsaka, T. *Electrochem. Commun.* **2005**, *7*, 29.
(50) Jasin, D.; Abu-Rabi, A.; Mentus, S.; Jovanovic, D. *Electrochim. Acta* **2007**, *52*, 4581.

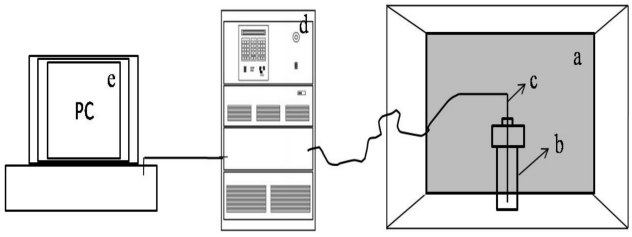

Figure 1. Schematic illustration of MW-HT setup: (a) microwave oven; (b) Teflon autoclave; (c) thermocouple; (d) temperature and power displayer; (e) computer.

Pt-based catalysts. Many efforts have been made to develop new catalysts.[49–52]

The objective of the present work was to prepare α-$Ni(OH)_2$ with enhanced electrochemical activity for the reduction of O_2 to OH^-. In this study, hydrothermal methods with assistance of microwave radiation in the presence of the urea were used for the synthesis of phase pure 3D flowerlike α-$Ni(OH)_2$ materials. We investigated the effects of the nickel sources, precipitators, and microwave irradiation. A possible growth mechanism for the 3D flowerlike α-$Ni(OH)_2$ is proposed in this paper. Rotating disk voltammetry (RDV) was applied to investigate kinetics of the oxygen reduction reaction. The Levich equation was used to calculate the number of electrons transferred in the oxygen reduction reaction.

2. Experiment Section

2.1. Synthesis of α-$Ni(OH)_2$. All reagents were analytical grade. The microwave oven used in this study was an MMT model 10 with the power range of 0–1200 W, and a thermocouple was inserted into the solution to monitor the temperature of the reaction. The schematic illustration is shown in Figure 1. In a typical experiment, 0.93 g of $Ni(NO_3)_3 \cdot 6H_2O$ and 0.19 g of urea were dissolved in 16 mL of distilled water and 16 mL of ethanol in a Teflon-lined autoclave with a 50 mL capacity which was transparent to microwave irradiation. A clear solution was obtained after stirring for 15 min. The autoclave was sealed and placed in the microwave oven being heated at 90 °C for 15 min. The autoclave was allowed to cool to room temperature naturally after the heat treatment. The resulting light green products were filtered, washed with distilled water and absolute ethanol, and then dried in the oven at 80 °C overnight. The sample became dark after calcining at 450 °C for 3 h.

2.2. Characterization. *2.2.1. Structure.* The crystal structure of the sample was determined by X-ray diffraction (XRD) analysis using a Scintag XDS 2000 diffractometer with Cu Kα radiation with a 1.5418 Å wavelength. A beam voltage of 45 kV and a 40 mA current beam were used.

2.2.2. Morphology. Morphologies of the samples were investigated using a Zeiss DSM 982 Gemini field-emission scanning electron microscope (FESEM) with a Schottky emitter. Powder samples were dispersed in ethanol and dropped onto a gold-coated silicon wafer, and then the wafer was then mounted onto a stainless steel sample holder using a silver conductive paint. High-resolution transmission electron microscopy (HRTEM) was also used to check the morphology of the samples. HRTEM studies were carried out on a JEOL 2010 instrument with an accelerating voltage of 200 kV. The samples were prepared by dispersing the material in 2-propanol. Then a drop of the dispersion was placed on a carbon-coated copper grid and allowed to dry.

2.2.3. IR. Fourier transform infrared (FTIR) spectra were recorded for a KBr diluted sample using a Nicolet Magna 750 IR spectrometer.

2.2.4. Thermal Stability. The thermal stability of the materials was studied by performing thermogravimetric analyses (TGA) and temperature-programmed desorption (TPD) with a mass spectroscopic detector. TGA was performed on a Hi-Res TGA 2950 thermogravimetric analyzer with 60 mL/min of N_2 flow from 25 to 700 °C at a heating rate 10 °C/min. In order to check the gas products evolved from the TGA experiment, temperature-programmed desorption (TPD) experiments were carried out. TPD data were collected in an apparatus specifically constructed for such measurements and equipped with an MSS-RGA mass spectroscopy detector (MKS instrument). About 50 mg of sample was loaded in a quartz tube and degassed at 40 mL/min. He was flowed at room temperature for 1.5 h and then at 100 °C for 2 h. After the pretreatment, the system was heated in a 40 mL/min He flow rate at a heating rate of 10 °C/min from 25 to 600 °C.

2.2.5. Electrocatalytic Activity. Cyclic voltammetry was used to test the electrocatalytic activity of α-$Ni(OH)_2$. A gas-diffusion electrode was prepared to check the ability of α-$Ni(OH)_2$ to reduce oxygen by CV. The process for the preparation of the electrode was shown in ref 53. The cell setup consisted of a sample mixture on carbon paper as the working electrode, an SCE reference electrode, a Pt counter electrode, and a 1.0 M KOH solution as the electrolyte. A computer-controlled CHI 430 electrochemical workstation was used to obtain cyclic voltammograms, and a scan rate of 50 mV/s was used. In a typical experiment, the cell was first purged with N_2(g) for 30 min followed by an initial scan, and then the cell was purged with O_2(g) for 30 min and scanned again. The reduction of H_2O_2 was applied to test the activity of the α-$Ni(OH)_2$ electrode. The same experimental conditions were used except that O_2 was absent in the system, and 0.1 mM H_2O_2 was added in the electrolyte.

To investigate the kinetics of α-$Ni(OH)_2$ toward oxygen reduction reaction, a Pine Instruments rotating electrode was used for rotating disk voltammetry (RDV) at a scan rate of 8.5 mV s^{-1}. The cell setup was the same as mentioned above, except that a pyrolytic graphite (PG, Advanced Ceramics, $A = 0.16$ cm^2) electrode was used as working electrode. The PG electrode was abraded with 400 grit SiC paper and was then cast with 30 μL of α-$Ni(OH)_2$ dispersed in water, which was allowed to dry overnight. Currents, where slight maxima occurred in RDV, were taken as the limiting currents. O_2 was purged for 30 min before each scan. All experiments were at ambient temperature (22 ± 2 °C).

3. Results

3.1. XRD. X-ray diffraction (XRD) was used to study the phase purity of the obtained nickel hydroxide as shown in Figure 2. All of the reflections in the XRD pattern in Figure 2b were consistent with the pattern reported for nickel nitrate hydroxide[54] which matched well with the standard pattern (JCPDS card: 22-752), as shown in Figure 2a. On the basis of the general formula of α-$Ni(OH)_2$, $[Ni(OH)_{2-x}A^{n-}_{x/n} \cdot yH_2O]$ with $x = 0.2$–0.4, $y = 0.6$–1, and A = Cl^-, NO_3^-, SO_4^{2-}, CO_3^{2-}, or OCN^-, the product prepared in the study was definitely the α-form. The first two peaks at 12.6° and 25.4°

(51) Shao, M. H.; Adzic, R. R. *J. Phys. Chem. B* **2005**, *109*, 16563.
(52) Schmidt, T. J.; Stamenkovic, V.; Arenz, M.; Markovic, N. M.; Ross, P. N. *Electrochim. Acta* **2002**, *47*, 3765.
(53) Crisostomo, V. M. B.; Ngala, J. K.; Alis, S.; Dobley, A.; Morein, C.; Chen, C.-H.; Shen, X.; Suib, S. L. *Chem. Mater.* **2007**, *19*, 1832.
(54) Rajamathi, M.; Kamath, P. V. *J. Power Sci.* **1998**, *70*, 118.

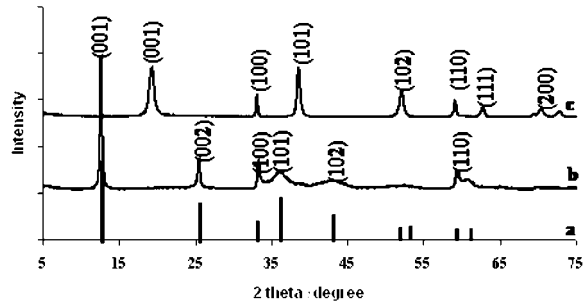

Figure 2. XRD patterns of (a) JCPDS card: 22-752, (b) α-Ni(OH)$_2$ prepared in this study, and (c) β-Ni(OH)$_2$ from Sigma-Aldrich.

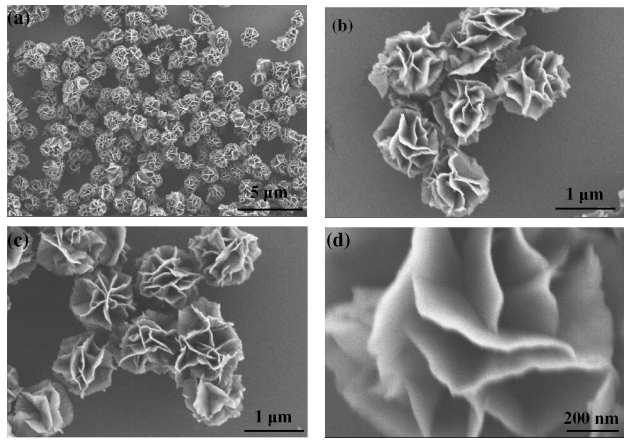

Figure 3. FE-SEM images of α-Ni(OH)$_2$ at different magnifications.

corresponded to the (001) and (002) planes, respectively. All the *d* spacing for peaks of the sample synthesized in this paper could be indexed to those of the nitrated α-Ni(OH)$_2$ with a slight shift in the (001) and (002) peak positions. These shifts were attributed to the extent and type of the intercalated anions (CO_3^{2-}, OCN^- besides NO_3^-) in the Ni(OH)$_2$ lattice. No peaks from β-Ni(OH)$_2$ (as shown in Figure 2c) were observed in the XRD pattern, indicating that the precipitated powders were pure α-Ni(OH)$_2$ at the XRD detection level.

3.2. FE-SEM and HR-TEM. Both β-Ni(OH)$_2$ and α-Ni(OH)$_2$ preferred to form hexagonal platelike shapes, since they had a hexagonal crystalline structure. Very recently, flowerlike, needlelike, and hollow sphere β-Ni(OH)$_2$ have been synthesized, but none of the α-Ni(OH)$_2$ with unique morphologies were reported. The morphology of the α-Ni(OH)$_2$ was studied by field emission scanning electron microscopy (FESEM) and high-resolution transmission electron microscopy (HRTEM). Figure 3a shows the SEM images of a typical sample composed of many uniform flowerlike architectures with diameters of 700 nm−1 μm, and the yield was above 99%. A closer observation of the flowerlike nanostructures is shown in Figure 3b,c, which indicated that each flower was composed of dozens of flakelike nanopetals. These nanopetals with around 20 nm thickness (as shown in Figure 3d) were connected to each other to build the 3D flowerlike structure. Figure 4a,b shows the TEM images of α-Ni(OH)$_2$ which are in good agreement with the results from SEM.

In addition, under SEM magnification, the nanopetals which are used to build up the 3D flower shapes have smooth

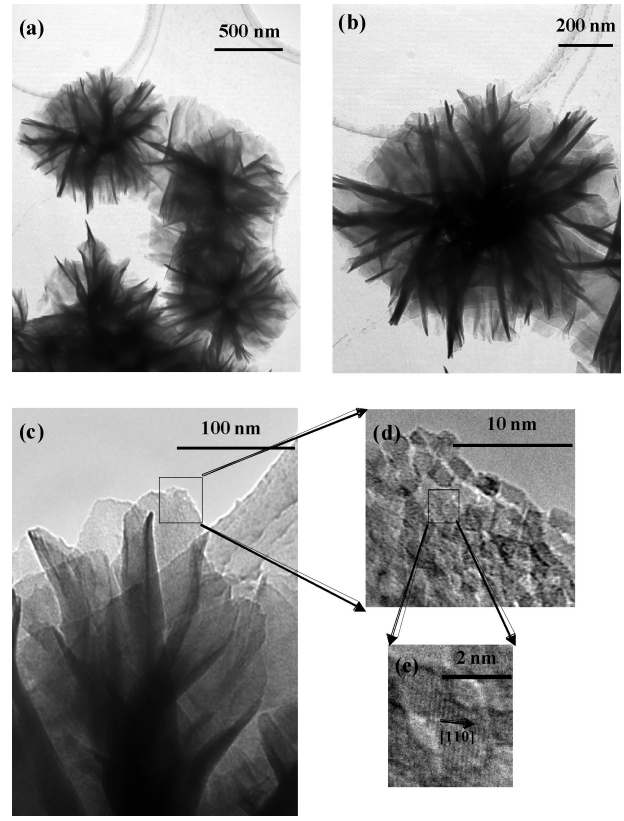

Figure 4. HRTEM images of α-Ni(OH)$_2$. Lattice fringes of the (110) planes are clearly shown in (e).

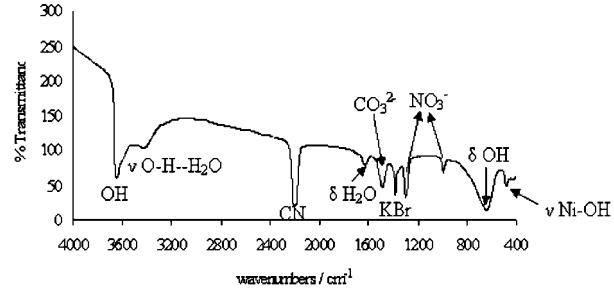

Figure 5. IR pattern of α-Ni(OH)$_2$.

surfaces, but on the basis of the observation of HRTEM, the petals have rough surfaces and consist of nanoparticles with 2–3 nm diameters, as shown in Figure 4b,c. The distances between the lattice fringes of the nanoparticles were around 1.6 Å, which corresponded to the *d* spacings of the (110) planes of α-Ni(OH)$_2$, confirming the formation of α-Ni(OH)$_2$, which was consistent with the XRD result.

3.3. FT-IR. The infrared spectrum of α-Ni(OH)$_2$ is shown in Figure 5. This spectrum shows the typical features of α-Ni(OH)$_2$. A narrow band located around 3647 cm^{-1} is due to the OH groups in the brucite-like structure. A broad band at 3460 cm^{-1} corresponds to the O−H vibration of a hydrogen-bonded water molecule which exists in the interlamellar space of α-Ni(OH)$_2$.[55] The very strong absorption band at 2202 cm^{-1} is the typical vibration of C≡N triple bonds in the OCN^- anions.[9] The band around 1630 cm^{-1} is assigned to the bending mode of the interlayer water

(55) Goler-Illia, G. J. de A. A.; Jobbágy, M.; Regazzoni, A. E.; Blesa, M. A. *Chem. Mater.* **1999**, *11*, 3140.

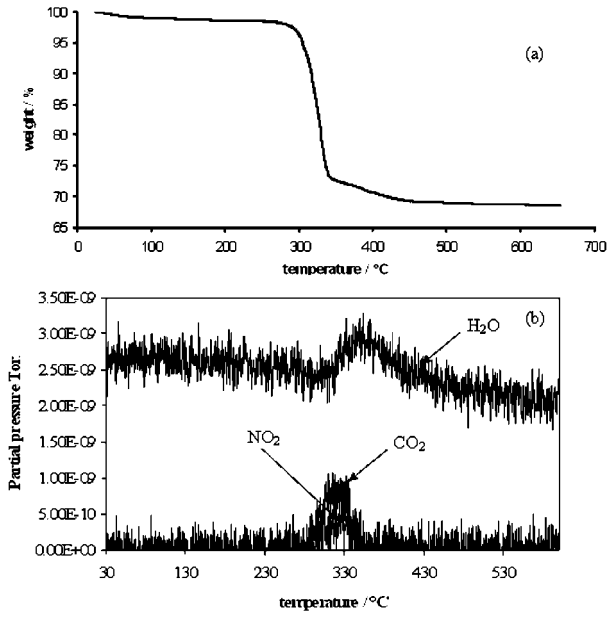

Figure 6. TGA (a) and TPD (b) plots in the N_2/He atmosphere.

molecule. The absorption around 1490 cm^{-1} is attributed to the carbonate ions. The presence of the 1385 cm^{-1} band is due to the interaction of the sample with the KBr in the pellet.[56] The bands at 1301 and 995 cm^{-1} are attributed to nitrate groups. The bands around 640 and 483 cm^{-1} are due to the δ_{OH} and ν_{Ni-OH} vibrations individually.[10] The results of FT-IR provided evidence for the presence of intercalated OCN^- and carbonate which were the byproducts of urea hydrolysis.[9]

3.4. Thermal Stability. The TGA curve of the α-$Ni(OH)_2$ is shown in Figure 6a. There were three main weight loss regions with a net weight loss of 32%. Figure 6b indicated the evolution of H_2O, NO_2, and CO_2 from α-$Ni(OH)_2$, which took place during the heat treatment under a He atmosphere with the same temperature ramp of 10 °C/min as that used in the TGA experiments. The He atmosphere results, which were used in the TPD experiments, should be similar to those obtained in the TGA experiments with N_2 because both He and N_2 are inert gases for α-$Ni(OH)_2$.

H_2O evolution was not observed in the TPD experiment when the temperature was lower than 100 °C because the sample in the TPD experiment was pretreated at 100 °C. The weight loss below 100 °C in the TGA experiment should be due to the removal of adsorbed water and the structurally bonded water.[44] Combining TGA and TPD data led to the conclusion that there was a 25% weight loss of α-$Ni(OH)_2$ in the range of 280 and 340 °C, which was due to the evolution of H_2O, NO_2, and CO_2. These gases corresponded to the decomposition products of α-nickel hydroxide and the intercalated anions, such as NO^{3-}, OCN^-, and CO_3^{2-}, which were confirmed by FT-IR. The existence of the intercalated ions also proved the formation of α-$Ni(OH)_2$, since there were not any interlayer ions in the β-$Ni(OH)_2$. Decomposition of hydroxide continued up to 450 °C which caused a 5% weight loss. The end product of TGA was pure NiO, which was confirmed by XRD experiments, and NiO still retained the morphology of α-$Ni(OH)_2$, as shown in Figure 7.

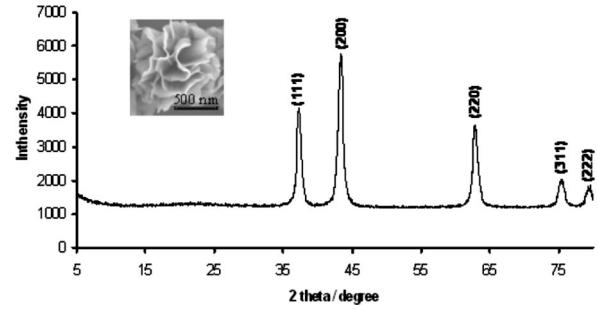

Figure 7. SEM and XRD pattern of α-$Ni(OH)_2$ after being calcined at 450 °C for 3 h.

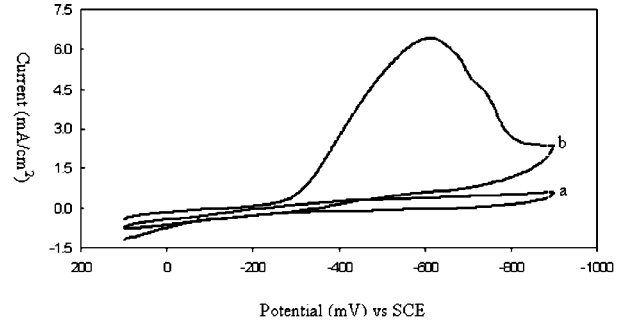

Figure 8. Cyclic voltammograms of α-$Ni(OH)_2$ obtained at a rate of 50 mV/s: (a) in N_2; (b) in O_2.

3.5. Electrocatalytic Activity. Figure 8 shows cyclic voltammograms for α-$Ni(OH)_2$. The voltammogram obtained in a N_2 atmosphere showed that α-$Ni(OH)_2$ was electrochemically inactive in this potential range and for the scan rate used in this experiment, as shown in Figure 8a. After saturation of the electrolyte with O_2, oxygen reduction potentials and peak currents were obtained, as shown in Figure 8b. The reduction peak potential vs SCE for the sample was −623 mV, which was in the region expected for a four-electron reduction of O_2 in eq 1:

$$2H_2O(l) + O_2(g) + 4e^- \rightarrow 4OH^-(l) \qquad (1)$$

When the electrolyte was repurged with O_2, α-$Ni(OH)_2$ showed a restoration of the O_2 reduction peak which meant that α-$Ni(OH)_2$ was stable toward O_2 reduction. On the basis of electrocatlytic activity results obtained from CV, battery properties of α-$Ni(OH)_2$ are now under investigation.

4. Discussion

4.1. Effects of Nickel Sources and Precipitators on the Crystal Phase and Morphology. In order to investigate which factors played critical roles in the synthesis of 3D flowerlike α-$Ni(OH)_2$, variations of the nickel source and precipitators have been made. In these experiments, nickel chloride was used as a nickel source instead of nickel nitrate. Figure 9 displays the powder XRD patterns of nickel hydroxide prepared from nickel chloride. All of the peaks in the pattern indicated the formation of the α-phase.[10] No peaks due to β-$Ni(OH)_2$ were observed in the XRD pattern.

(56) Rajamathi, M.; Kamath, P. V. *J. Power Sources* **1998**, *70*, 118.

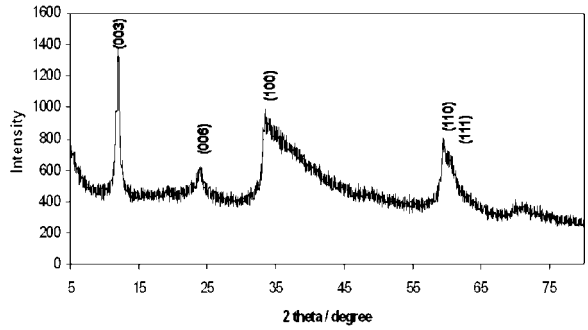

Figure 9. XRD pattern of the sample synthesized from $NiCl_2$.

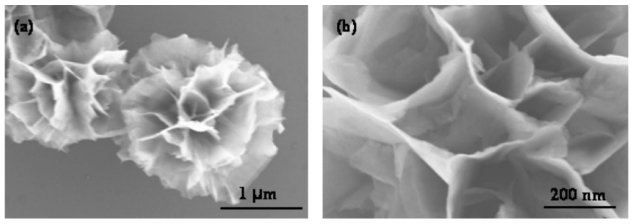

Figure 10. FE-SEM images of the sample obtained from $NiCl_2$.

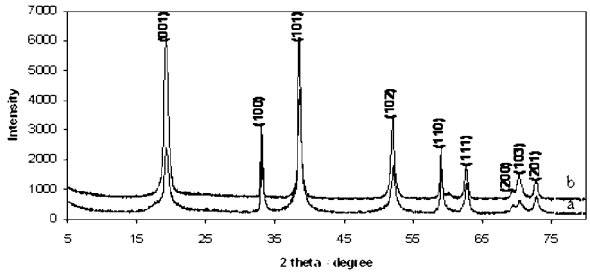

Figure 11. XRD patterns obtained for different precipitators: (a) NaOH and (b) $NH_3 \cdot H_2O$.

On the basis of the pattern shown in Figure 2, the sample obtained from nickel nitrate had better crystallinity than the product in the nickel chloride system and also showed a slight shift of the interlamellar spacing which was caused by the different intercalated anions, NO_3^- and Cl^-. The asymmetry of the reflection around 35° indicates the formation of a turbostratic phase. Nickel sources did not significantly affect the formation of α-phase nickel hydroxide. The morphology of this kind of α-$Ni(OH)_2$ still remained as flowerlike shapes but had thinner flakes, as shown in Figure 10, as compared with those shown in Figure 3d.

The nature of the precipitating agent had a large influence on the properties of the eventual product.[57] In this work the effects of precipitators were studied. Sodium hydroxide and ammonia were used in place of urea, while other conditions were kept the same. XRD patterns in Figure 11 showed that pure β-phase nickel hydroxide (JCPDS 14-117) was prepared rather than α-$Ni(OH)_2$. The morphologies were different from those of α-$Ni(OH)_2$. β-$Ni(OH)_2$ had a flakelike morphology but different size due to the use of a different kind of precipitator, as shown in Figure 12.

On the basis of the above investigation, precipitators played an important role in the formation of α-$Ni(OH)_2$. Urea

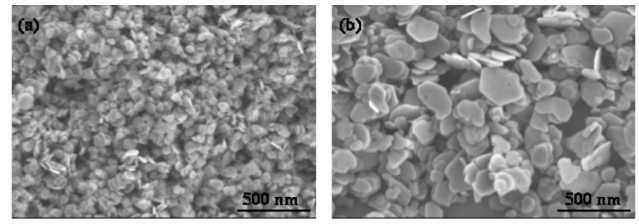

Figure 12. FE-SEM images obtained for different precipitators: (a) NaOH and (b) $NH_3 \cdot H_2O$.

was very critical for obtaining flowerlike α-$Ni(OH)_2$. There are many previous studies to investigate what happened to urea during the precipitation process. Li[16] claimed that NH_3 and CO_2 were obtained around 70 °C after the decomposition of urea. Then OH^- and CO_3^{2-} were produced by the hydrolysis of NH_3 and CO_2. A byproduct produced in the urea hydrolysis, which was OCN^-,[10] is confirmed by FT-IR experiments. The main reactions in the system are shown in the following equations:

$$H_2NCONH_2(s) + HO_2(l) \rightarrow 2NH_3(g) + CO_2(g) \quad (2)$$

$$CO_2(g) + HO_2(l) \rightarrow CO_3^{2-}(l) + 2H^+(l) \quad (3)$$

$$NH_3(g) + HO_2(l) \rightarrow NH_4^+(l) + 2OH^-(l) \quad (4)$$

$$H_2NCONH_2(s) + HO_2(l) \rightarrow NCO^-(l) + NH_4^+(l) \quad (5)$$

Urea provided a steady OH^- ion supply via hydrolysis.[58] The reaction between the nickel ions and OH^- ions was controllable, which might be why α-$Ni(OH)_2$ was formed. When sodium hydroxide or ammonia was added directly to nickel solution, precipitation occurred. The pH value of the solution was quite different after the reaction. For urea hydrolysis, the final pH was around 6.8; however, the pH of the solution in sodium hydroxide or ammonia was around 13. β-$Ni(OH)_2$ is the preferred product in a strong alkaline solution. Thus, α-$Ni(OH)_2$ only could be synthesized in the presence of urea under these experimental conditions.

In this study, temperature-dependent experiments have been done. The samples were collected at different temperatures: 80, 100, 110, and 120 °C. After the XRD and SEM measurements, we found either a crystalline phase or that the morphology had not changed. Temperature is not critical in this experiment when the temperature was higher than the urea hydrolysis point (above 60 °C), since no sample was obtained when the temperature was lower than 60 °C.

4.2. Microwave Effect. Many studies have investigated the role of microwave irradiation in the synthesis of inorganic materials.[25–29] In this study the conventional hydrothermal (HT) method was used to compare results with those obtained with the microwave hydrothermal (MW-HT) method. In HT, the reactant ratios and reaction temperatures were kept constant with MW-HT, but the reaction times were prolonged to 10 h, since we could not collect any sample after 15 min of reaction. Because of the high penetration depth of microwave heating, the heating was rapid, which caused an increase in reaction kinetics. The XRD patterns, displayed

(57) Acharya, R.; Subbaish, T.; Anand, S.; Das, R. P. *Mater. Lett.* **2003**, *57*, 3089.

(58) Zhong, L.-S.; Hu, J.-S.; Liang, H.-P.; Cao, A.-M.; Song, W.-G.; Wan, L.-J. *Adv. Mater.* **2006**, *18*, 2426.

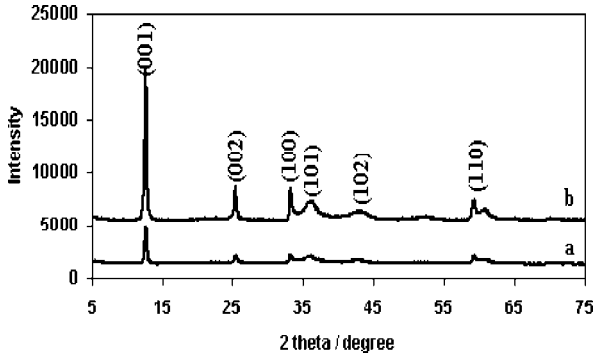

Figure 13. XRD patterns of the samples prepared by (a) conventional HT and (b) MW-HT.

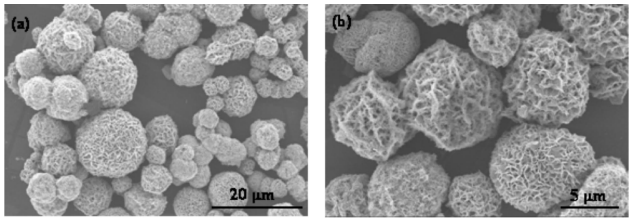

Figure 14. FESEM images of the samples prepared by conventional hydrothermal method at different magnifications.

in Figure 13, showed that α-$Ni(OH)_2$ was obtained by HT, but the intensities of the peaks were much weaker than those of the sample prepared by MW-HT. Therefore, the enhancement of crystallinity performed in short periods via microwave treatment could be attributed to fast heating of the precursor due to avoidance thermal gradients.[36]

On the basis of FE-SEM images, microspheres with different sizes were observed; the sizes varied from 3 to 10 μm (as shown in Figure 14). Compared to the images shown in Figure 4, the morphologies and particle sizes of the samples synthesized by MW-HT were much more homogeneous than those of samples prepared by conventional HT methods. The differences in the obtained samples between MW-HT and conventional HT methods can be seen in the different XRD peak intensities, different morphologies, and particle sizes.

Microwaves are nonionizing electromagnetic radiation; they produced dipole reorientation or ionic conduction when they interact with materials that are dielectric materials or in which there are ions. Uniform heating in these materials is favored, which led to the homogeneous shapes and particle sizes. MW-HT methods also led to enhanced crystallinity of α-$Ni(OH)_2$. Benito et al.[59] found microwave radiation could improve the crystallinity of LDHs with compositions of Mg, Al-CO_3 and Mg, Cr-CO_3. Microwave hydrothermal synthesis has major advantages over conventional hydrothermal methods in terms of an increase of reaction kinetics, decreased energy savings, shorter processing times, uniformity of the samples, and improvement of crystallinity.

4.3. Possible Growth Mechanism of the Flowerlike α-$Ni(OH)_2$. As shown in Figure 4, the α-$Ni(OH)_2$ self-assembled into a flower morphology consisting of flakes. In order to understand the evolution process of the 3D flowerlike α-$Ni(OH)_2$ material, time-dependent experiments were carried out, during which the samples were collected at different times after the temperature reached 90 °C. As shown in Figure 15a, the sample collected at 1 min consisted of very thin flakes. The samples obtained 5 min later (Figure 15b) showed the flakes were getting thicker, and there was some aggregation of flakes to form a flowerlike morphology. As the reaction proceeded (Figure 15c), no single flakes remained. All of the flakes transformed into 3D flowers.

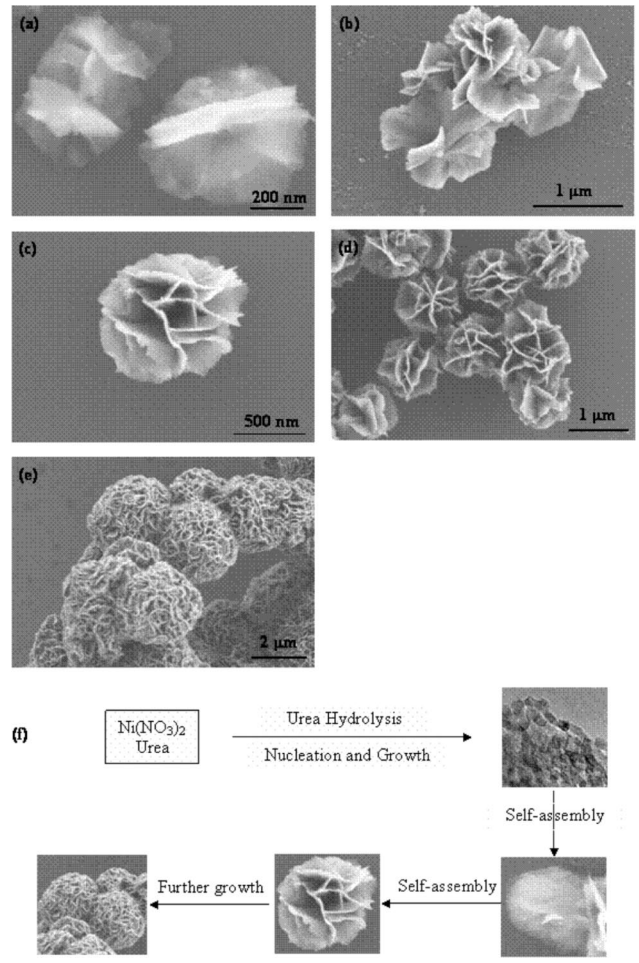

Figure 15. FESEM images of the samples collected at different times after the temperature reached 90 °C: (a) 1, (b) 5, (c) 10, (d) 15, and (e) 120 min. (f) Schematic explanation of the morphological evolution of α-$Ni(OH)_2$.

With an extension of reaction time, the morphologies and the sizes of the particles still remained the same but the yield increased, as shown in Figure 15d. Figure 15e shows the images of the sample obtained at 2 h. The aggregation of the flakes is enhanced, and microspheres were produced. From this point, the sizes and the morphologies of the product remained the same when the reaction time was less than 2 h. As the reaction proceeds, the microspheres are the main morphology. The reaction under microwave irradiation heating was very fast. Therefore, it is hard to collect the sample before flakes were produced. However, high-resolution TEM (Figure 4d) data provided evidence that the flakes were composed of nanoparticles. We illustrate this evolution process in

(59) Benito, P.; Labajos, F. M.; Rocha, J.; Rives, V. *Microporous Mesoporous Mater.* **2006**, *94*, 148.
(60) Liu, B.; Zeng, H. C. *J. Am. Chem. Soc.* **2004**, *126*, 8124.

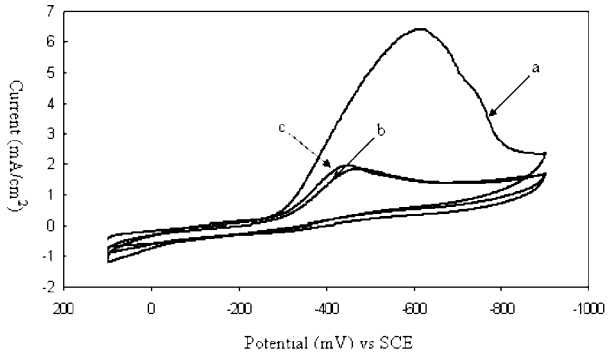

Figure 16. Cyclic voltammograms of α-Ni(OH)$_2$ prepared by different methods: (a) MW-HT, (b) conventional HT method, and (c) β-Ni(OH)$_2$ prepared with $NH_3 \cdot H_2O$ as precipitator.

Figure 15f. The XRD pattern indicated that the flowerlike α-Ni(OH)$_2$ had good crystallinity; however, HR-TEM showed that the nanopetals of the flower were composed of nanaparticles with 2–3 nm diameters. There is an ordered superstructure from the arrangement of nanoparticles.

The precursor of the species nucleated to form tiny single crystals (2–3 nm), as proposed previously.[32] These single crystals then aggregated and formed flakes. As the reaction continues, these flakes self-organize into 3D flowerlike structures. Many forces cause the flakes to self-assemble into the flowerlike morphology, such as electrostatic and dipolar fields associated with the aggregate, hydrophobic interactions, hydrogen bonds, crystal-face attraction, and van der Waals forces. In this case, hydroxyl defects in the Ni(OH)$_x$ layer resulted in a positive charge of the layer. Because of the existence of OH^- groups, electrostatic and hydrogen bonds might be the main driving forces for self-assembly. Such a process was similar to that in a previous report in which CuO microshperes were built from small crystal strips that contained even smaller one-dimensional nanoribbons.[60] Zhong[58] described the evolution mechanism of a flowerlike iron oxide precursor in the presence of CTAB, which followed Ostwald ripening kinetics. In our study, under microwave irradiation heating there was no observation about expansion of small particles to form flakes or flowers. However, the nanocrystals aggregated to form flakes.

Figure 16 shows the cyclic voltammograms for α-Ni(OH)$_2$ prepared by different methods and β-Ni(OH)$_2$ prepared when $NH_3 \cdot H_2O$ was used as precipitator. Peak currents are used to measure the electrocatalytic activity of manganese oxides.[61] The method that Mao et al.[61] used to determine the peak current from CV was applied in our study. α-Ni(OH)$_2$ prepared by the MW-HT method which shows the highest current peak has the best electrocatalytic activity to the electrochemical reduction of O_2 among three samples. The O_2 reduction potentials shift from −623 mV to around −450 mV, which means different reactions of O_2 reduction take place on the electrode. The reactions on the (b) and (c) electrodes in Figure 17 are two-electron reductions of O_2 to HO_2^-, and the reaction on the (a) electrode might be a four-

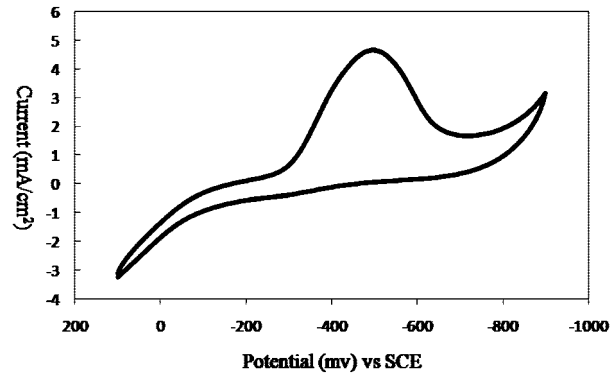

Figure 17. Cyclic voltammograms of α-Ni(OH)$_2$ in the presence of 0.1 mM H_2O_2.

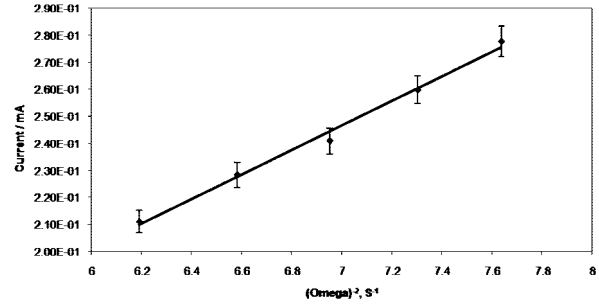

Figure 18. Square root of the rotation rates plotted against the limiting current.

electron reduction of O_2 to OH^-, eqs 6 and 7, as suggested in the literature.[62]

$$O_2 + 2e^- + H_2O \rightarrow HO_2^- + OH^- \quad (6)$$

$$HO_2^- + 2e^- + H_2O \rightarrow 3OH^- \quad (7)$$

Figure 17 shows the H_2O_2 reduction reaction in the absence of O_2; the electrolyte contains 0.1 mM H_2O_2 and was purged with N_2. A peak current reduction potential around 477 mV suggested there is catalytic activity of the α-Ni(OH)$_2$ electrode for H_2O_2 reduction to OH^-.

To investigate the number of electrons transferred in (a) electrode, an α-Ni(OH)$_2$ cast PG electrode was employed in RDV. According to the Levich equation[63]

$$i_L = 0.620nFAD_0^{2/3}\omega^{1/2}\nu^{-1/6}C_0^* \quad (8)$$

where i_L (A) is the limiting current for the electrode reaction of reactive species by a diffusion-controlled process, n (mol^{-1}) is the number of electrons transferred per mole of reactive species, F (96 500 C mol^{-1}) is the Faraday constant, A (cm^2) is the electrode area, D_0 (cm^2 s^{-1}) is the diffusion coefficient of O_2 in 1.0 M KOH solution (= 1.76×10^{-5} cm^2 s^{-1}), ω (s^{-1}) is the rotation rate, ν (cm^2 s^{-1}) is the kinetic viscosity of solution (= 0.01 cm^2 s^{-1}), and C_0* (mol cm^{-3}) is the concentration of O_2 in 1.0 M KOH solution at 298 K (= 1.103×10^{-6} mol cm^{-3}).[64] The square root of the rotation rates were plotted against the limiting current, as depicted in Figure 18. The number of electrons transferred was calculated to be 2.96, which is close to 3. This could

(61) Mao, L.; Sotomura, T.; Nakatsu, K.; Koshiba, N.; Zhang, D.; Ohsaka, T. *J. Electrochem. Soc.* **2002**, *149*, A504.
(62) Chang, C.; Wen, T. *Electrochim. Acta* **2006**, *52*, 623.
(63) Jiang, R. Z.; Chu, D. *Electrochim. Acta* **2000**, *45*, 4025.
(64) Jiang, R. Z.; Anson, F. C. *J. Electroanal. Chem.* **1991**, *305*, 171.

possibly be due to the concurrence of two-electron reactions as well as four-electron reactions, since further reduction can be prevented by the diffusion of the two-electron reaction product. So we could draw the conclusion that O_2 can fulfill a four-electron reduction on the α-$Ni(OH)_2$ electrode.

Compared with α-$Ni(OH)_2$ prepared by conventional HT methods, α-$Ni(OH)_2$ synthesized by MW-HT has 3D flowerlike morphologies and smaller particle sizes which might have a strong influence on the electrochemical performance of the α-$Ni(OH)_2$.

5. Conclusions

The microwave hydrothermal method is an effective method for preparation of α-$Ni(OH)_2$. Compared to conventional hydrothermal methods, MW-HT was better due to use of low-energy, time-saving, enhanced crystallinity, homogeneous morphologies, and uniform particle sizes. The obtained α-$Ni(OH)_2$ had uniform 3D flowerlike shapes composed of aggregates of flakes which are built from nanocrystals. TEM studies confirmed the growth mechanism of the flowerlike morphology. FT-IR results and TPD experiments showed the existence of intercalated ions. α-$Ni(OH)_2$ exhibited good electrochemical performance. In the process of preparing pure phase and flowerlike α-$Ni(OH)_2$, nickel sources did not have much influence, but urea played a crucial role. Flowerlike morphologies and nanosized particles enhanced the electrochemical activity of α-$Ni(OH)_2$ for the electrochemical reduction of O_2. CV experiments and rotating disk voltammetry showed that O_2 might be a four-electron reduction on the α-$Ni(OH)_2$ electrode.

Acknowledgment. We thank NSF NIRT for the support of this work (award CTS-0304217). We thank Dr. Aindow for access to the JEOL 2010 TEM instrument in the Institute of Materials Science and Dr. Jim Romanow for the help with FESEM experiments in the Physiology and Neurobiology Department. We acknowledge Dr. Francis S. Galasso for helpful discussions. We also thank Dr. Ahbay Vaze for help with CV experiments.

CM702207W